Medicinal Chemistry Research
https://doi.org/10.1007/s00044-018-2160-6

MEDICINAL CHEMISTRY RESEARCH

ORIGINAL RESEARCH

Collection of alkenylcoumarin derivatives as *Taq* DNA polymerase inhibitors: SAR and in silico simulations

Ezequiel Bruna-Haupt[1] · Hugo A. Garro[1] · Lucas Gutiérrez[2] · Carlos R. Pungitore[1]

Received: 17 December 2017 / Accepted: 20 February 2018

Abstract

Using a feasible method, we generated a small focused library of structurally related alkenylcoumarins. These compounds were evaluated as potential antitumoral agents against *Taq* DNA polymerase. 6-(pent-4-enyloxy)-coumarin (**7**) $IC_{50} = 48.33 \pm 2.85$ μM was defined as a small molecule able to disturb DNA replication. Docking and Molecular Dynamic Simulations suggest an active-site binding. Structure/activity relationship was reasonably established. Compound **7** represents a potential structure for further studies in the development of new anti-cancer DNA/polymerase binding agents.

Keywords DNA polymerase · Antitumoral · SAR · Coumarin · Natural Products

Introduction

DNA polymerases are vital enzymes that govern the cell cycle and are involved in the synthesis of genetic material from one organism and the transfer of all the processes of cell division. DNA polymerases inhibition affects the unlimited replicative potential of cancer cells, and consequently antitumoral activity. There is a close evolutionary relationship between human DNA polymerases and *Taq* DNA polymerase (Pungitore 2014; Garro et al. 2015a). Natural and synthetic coumarins exhibit exceptional pharmacological properties, such as antibiotic, antiviral, anti-HIV, anticoagulant, and antitumoral (Stefanou et al. 2011; Garro et al. 2014a; Venugopala and Odhav 2013; Olmedo et al. 2012; Kostova et al. 2006). The search for pharmacophores involves indispensable structural aspects in the molecules capable of binding specific protein receptors and then developing pharmacological activities. This can be done using combinatorial chemistry, which permits to produce quickly new collections of compounds of various sizes and compositions, thus increasing molecular diversity, sometimes in a random and expensive manner (Wijkmans and Beckett 2002). Fragment-based drug design (FBDD) involves the experimental screening of libraries of small chemical fragment, via in silico studies of virtual fragments if the structural information of the target is available (Liu et al. 2017). A more rational method could involve subtle changes using homologous series of related chemical substituent (Ghiano et al. 2017; Rayati and Nejabat 2016). Simulation studies using computational chemistry allow the investigation of molecular properties like flexibility, distortion, stabilization of protein/ligand complexes due to the physicochemical interactions between them (Bernauer et al. 2007; Li 2012).

It has been evaluated that simple structural differences between the products obtained after modification of natural coumarins moieties determine substantial changes in their activity and selectivity as inhibiting agents. This bioactivity difference is often obtained by mild structural modifications, either by the presence of a hydroxyl group or a methyl group, or both, at specific positions inside the coumarin core (Garro and Pungitore 2015b; Garro et al. 2014b; Kostova 2007).

The objective of this paper was to generate a collection of structurally related alkenylcoumarins with subtle differences in long chain chemical groups and their positions in the coumarin core. Taking account our previous work

Electronic supplementary material The online version of this article (https://doi.org/10.1007/s00044-018-2160-6) contains supplementary material, which is available to authorized users.

✉ Hugo A. Garro
hugocanaya@yahoo.com.ar
hgarro@unsl.edu.ar

[1] Área de Química Orgánica, INTEQUI-CONICET-UNSL, San Luis 5700, Argentina

[2] Facultad de Química, Bioquímica y Farmacia, Universidad Nacional de San Luis, IMIBIO-SL (CONICET), Chacabuco 915, San Luis 5700, Argentina

Published online: 07 March 2018

(Garro et al. 2014a) in which some allylic coumarins were shown to be active against DNA related enzymes, we proceeded to investigate the activity of new derivatives against *Taq* DNA polymerase and their potential in the search for possible pharmacophores using mainly simulation methods.

Materials and methods

General procedure for coumarin derivatives synthesis

150 mg (0.926 mMol) of 6-hydroxy (**1**), 7-hydroxy (**2**), or 4-hydroxycoumarin (**3**) separately were dissolved in 4 ml of DMF, with 36 mg (1.5 Eq) of NaH and 2 Eq. of 4-penten, 3-buten, *trans*-crotyl, allyl or *γ,γ*-dimethylallyl bromide. Similarly, 2 Eq. of 1-bromide-3-methylbutane were employed with 150 mg (0.926 mMol) of 7-hydroxycoumarin with 36 mg (1.5 Eq) of NaH. The reaction mixture was stirred at 0 °C for 15 min, then brought to a temperature below the boiling point of the DMF (153 °C) for another 15 min, and finally stirred at room temperature for 24 h, in order to favor the displacement of kinetic and thermodynamic equilibrium towards product formation. The crude reaction product was then partitioned with diethyl ether, a saturated solution of NaCl (brine) at room temperature and two washes with water at 5 °C. The organic layer was washed several times with distilled water and then dried with anhydrous Na_2SO_4. The vacuum evaporation residue was purified by silica gel column chromatography, using distillated *n*-Hexane/AcOEt mixtures at increasing polarities. The isolated compounds were analyzed by HRMS, ESI-MS ^{1}H-NMR, ^{13}C-NMR and bidimensional experiments like DEPT, H,H-COSY and HETCOR.

Spectroscopy data for compounds 4–18

6-allyloxy-coumarin (4)

75% yield. ^{1}H NMR (200 MHz $CDCl_3$, p.p.m.) *δ*: 4.55 (d, 2H, CH_2), 5.2–5.5 (m, 2H, allyl-CH_2), 5.9–6.2 (m, 1H, allyl-CH), 6.4 (d, $J = 9.6$ Hz, 1H, lactone-H), 6.9 (br s, 1H, ArH), 7.15 (d, 1H, ArH), 7.25 (d, 1H, ArH), 7.65 (d, $J = 9.6$ Hz, 1H, lactone-H). ^{13}C NMR (50.6 MHz, $CDCl_3$, p.p.m.) *δ*: 160.92, 155.03, 148.52, 143.18, 132.69, 120.07, 119.16, 118.08, 117.83, 117.06, 111.26, 69.47. ESI–MS: *m/z* 225.0534 (M + 23), Calc. for $C_{12}H_{10}O_3Na$: 225.0528

6-crotyloxy-coumarin (5)

63% yield. ^{1}H NMR (200 MHz $CDCl_3$, p.p.m.) *δ*: 1.75 (d, 2H, CH_3 mayor product attributable to *trans* configuration: $J = 7.2$ Hz; minor product attributable to *cis* configuration: $J = 4.9$ Hz), 4.55 (d, 2H, CH_2 mayor product attributable to *trans* configuration: $J = 5.8$ Hz; minor product attributable to *cis* configuration: $J = 5.8$ Hz), 5.6–5.8 (m, 1H, crotyl-CH), 5.8–6.0 (m, 1H, crotyl-CH), 6.4 (d, $J = 9.6$ Hz, 1H, lactone-H), 6.9 (br s, 1H, ArH), 7.1 (br d, 1H, ArH), 7.25 (d, 1H, ArH), 7.65 (d, $J = 9.6$ Hz, 1H, lactone-H). ^{13}C NMR (50.6 MHz, $CDCl_3$) 161.00, 155.15, 143.21, 131.17, 125.46, 120.10, 119.14, 117.11, 69.40, 17.85. ESI–MS: *m/z* 239.06748 (M + 23), Calc. for $C_{13}H_{12}O_3Na$: 239.06787

6-(but-3-enyloxy)-coumarin (6)

60% yield. ^{1}H NMR, (200 MHz $CDCl_3$, p.p.m.) *δ*: 2.55 (m, 2H), 4.05 (t, $J = 6.67$ Hz, 2H), 5.1–5.33 (m, 2H), 5.8–6.0 (m, 1H), 6.4 (d, $J = 9.5$ Hz, 1H, lactone-H), 6.9 (s, 1H, ArH), 7.1 (br d, 1H, ArH), 7.25 (d, 1H, ArH), 7.65 (d, $J = 9.5$ Hz, 1H, lactone-H). ^{13}C NMR (50.6 MHz, $CDCl_3$, p.p.m.) *δ*: 162, 155, 143.18, 134.06, 119.94, 119.17, 117.34, 117.09, 110.92, 67.95, 33.51. ESI–MS: *m/z* 239.06725 (M + 23), Calc. for $C_{13}H_{12}O_3Na$: 239.06787

6-(pent-4-enyloxy)-coumarin (7)

67% yield. ^{1}H NMR, (200 MHz $CDCl_3$, p.p.m.) *δ*: 1.9 (q, 2H), 2.25 (q, 2H), 4.0 (t, $J = 6.4$ Hz, 2H), 4.95–5.03 (br d, 2H), 5.7–6.0 (m, 1H), 6.4 (d, $J = 9.5$ Hz, 1H, lactone-H), 6.9 (d, 1H, ArH), 7.1 (br d, 1H, ArH), 7.2(s, 1H, ArH), 7.63 (d, $J = 9.5$ Hz, 1H, lactone-H). ^{13}C NMR (50.6 MHz, $CDCl_3$, p.p.m.) *δ*: 155.53, 148.37, 143.20, 137.54, 119.90, 119.15, 117.83, 115.41, 110.75, 67.86, 30.00, 28.28. ESI–MS: *m/z* 253.08309 (M + 23), Calc. for $C_{14}H_{14}O_3Na$: 253.08352

7-(γ,γ-dimethyl-allyloxy)-coumarin (8)

84% yield. ^{1}H NMR (200 MHz $CDCl_3$, p.p.m.) *δ*: 1.76 (s, 3H, CH_3), 1.80 (s, 3H, CH_3), 4.57 (d, $J = 6.8$ Hz, 2H, CH_2), 5.47 (t, $J = 6.8$ Hz, 1H, CH), 6.25 (d, $J = 9.8$ Hz, 1H, lactone-H), 6.86 (d, 1H, ArH), 6.87 (br s, 1H, ArH), 7.36 (d, 1H, ArH), 7.64 (d, $J = 9.8$ Hz, 1H, lactone-H). ^{13}C NMR (50.6 MHz, $CDCl_3$, p.p.m.) *δ*: 162.12, 155.85, 143.44, 139.38, 128.70, 118.66, 113.14, 112.91, 112.42, 101.56, 65.42, 25.78, 18.25. ESI–MS: *m/z* 253.0851 (M + 23), Calc. for $C_{14}H_{14}O_3Na$: 253.0834

7-crotyloxy-coumarin (9)

85% yield. ^{1}H NMR (200 MHz $CDCl_3$, p.p.m.) *δ*: 1.75 (d, 3H, CH_3 mayor product attributable to *trans* configuration: $J = 7.4$ Hz; minor product attributable to *cis* configuration: $J = 5.0$ Hz), 4.5 (2H, CH_2 mayor product attributable to *trans* configuration: $J = 5.9$ Hz; minor product attributable to *cis* configuration: $J = 6.1$ Hz), 5.6–5.8 (m, 1H, crotyl-

CH), 5.8–6.0 (m, 1H, crotyl-CH), 6.25 (d, $J = 9.5$ Hz, 1H, lactone-H), 6.8 (s, 1H, ArH), 6.87 (br s, 1H, ArH), 7.37 (d, 1H, ArH), 7.65 (d, $J = 9.5$ Hz, 1H, lactone-H). ^{13}C NMR (50.6 MHz, $CDCl_3$, p.p.m.) δ: 161.89, 161.15, 155.78, 143.36, 131.52, 128.66, 124.95, 113.09, 101.60, 62.20, 17.78. ESI–MS: *m/z* 239.06753 (M + 23), Calc. for $C_{13}H_{12}O_3Na$: 239.06787

7-(but-3-enyloxy)-coumarin (10)

68% yield. ^{1}H NMR (200 MHz $CDCl_3$, p.p.m.) δ: 2.6 (m, 2H, CH_2), 4.1 (t, $J = 6.66$ Hz 2H), 5.1–5.3 (br d, 2H, butilen-CH_2), 5.8–6.0 (m, 1H, CH), 6.23 (d, $J = 9.5$ Hz, 1H, lactone-H), 6.8 (d, 1H, ArH), 6.85 (br s, 1H, ArH), 7.36 (d, 1H, ArH), 7.6 (d, $J = 9.5$ Hz, 1H, lactone-H). ^{13}C NMR (50.6 MHz, $CDCl_3$, p.p.m.) δ: 162.09, 161.20, 155.82, 143.40, 133.76, 133.40, 112.92, 112.47, 101.34, 97.71, 33.26. ESI–MS: *m/z* 239.06954 (M + 23), Calc. for $C_{13}H_{12}O_3Na$: 239.06954

7-(pent-4-enyloxy)-coumarin (11)

61% yield. ^{1}H NMR (200 MHz $CDCl_3$, p.p.m.) δ: 1.8–2.0 (q, 2H), 2.2–2.43 (q, 2H), 4.03 (t, $J = 6.5$ Hz, 2H), 4.96–5.15 (br d, 2H), 5.75–6.0 (m, 1H), 6.25 (d, $J = 9.5$ Hz, 1H, lactone-H), 6.8 (s, 1H, ArH), 6.85 (br d, 1H, ArH), 7.36 (d, 1H, ArH), 7.63 (d, $J = 9.5$ Hz, 1H, lactone-H). ^{13}C NMR (50.6 MHz, $CDCl_3$, p.p.m.) δ: 162.25, 161.21, 155.83, 143.40, 137.33, 128.97, 115.48, 112.88, 112.37, 101.28, 67.70, 29.91, 28.01. ESI–MS: *m/z* 253.08339 (M + 23), Calc. for $C_{14}H_{14}O_3Na$: 253.08352

7-(3-methylbutane)-oxycoumarin (12)

64% yield. ^{1}H NMR (200 MHz $CDCl_3$, p.p.m.) δ: 0.98 (d, $J = 6.4$ Hz, 6H, 3-methylbutane-CH_3x2), 1.69–1.88 (m, 2H, 3-methylbutane-CH_2), 1.75–1.9 (m, 1H, 3-methylbutane-CH), 4.04 (t, $J = 6.6$ Hz, 2H, 3-methylbutane-CH_2), 6.23 (d, $J = 9.2$ Hz, 1H, lactone-H), 6.81 (s, 1H, ArH), 6.84 (d, 1H, ArH), 7.36 (d, 1H, ArH), 7.62 (d, $J = 9.2$ Hz, 1H, lactone-H).

7-allyloxy-coumarin (13)

70% yield: ^{1}H NMR (200 MHz $CDCl_3$, p.p.m.) δ: 4.6 (br d, 2H, allyl-CH_2), 5.3–5.5 (m, 2H, allyl-CH_2), 5,9–6,2 (m, 1H, allyl-CH) 6.25 (d, $J = 9.5$ Hz, 1H, lactone-H), 6.83 (br ds, 1H, ArH), 6.88 (d, 1H, ArH), 7.38 (d, 1H, ArH), 7.63 (d, $J = 9.5$ Hz, 1H, lactone-H). ^{13}C NMR (50.6 MHz, $CDCl_3$, p.p.m.) δ: 161.76, 161.17, 155.83, 143.55, 143.35, 128.73, 118.55, 113.20, 112.64, 101.73, 69.26. ESI–MS: *m/z* 225.0529 (M + 23), Calc. for $C_{12}H_{10}O_3Na$: 225.0528

4-O-crotyloxy-coumarin (14)

41% yield. ^{1}H NMR (200 MHz $CDCl_3$, p.p.m.) δ: 1.8 (d, 3H, crotyl-CH_3 mayor product attributable to *trans* configuration: $J = 7.41$ Hz; minor product attributable to *cis* configuration: $J = 5.12$ Hz), 4.6 (d, 2H, crotyl-CH_2 mayor product attributable to *trans* configuration: $J = 6.06$ Hz; minor product attributable to *cis* configuration: $J =$ 6.20 Hz), 5.65 (s, 1H, lactone-H), 5.7–5.85 (m, 1H, crotyl-CH), 5.8–6.1 (m, 1H, crotyl-CH), 7.25 (br dd, 1H, ArH), 7.55 (br dd, 1H, ArH), 7.85 (d, 1H, ArH), 7.85 (d, 1H, ArH). ^{13}C NMR (50.6 MHz, $CDCl_3$, p.p.m.) δ: 165.36, 162.99, 153.35, 132.83, 132.80, 132.31, 123.91, 123.13, 116.73, 90.75, 69.94, 17.87. ESI–MS: *m/z* 239.06815 (M + 23), Calc. for $C_{13}H_{12}O_3Na$: 239.06787

4-hydroxy-3-C-crotyl-coumarin (15)

30% yield. ^{1}H NMR (200 MHz $CDCl_3$, p.p.m.) δ: 1.76 (d, 3H, crotyl-CH_3 mayor product attributable to *trans* configuration: $J = 7.65$ Hz; minor product attributable to *cis* configuration: $J = 4.82$ Hz), 3.45 (d, 2H, crotyl-CH_2 mayor product attributable to *trans* configuration: $J = 6.48$ Hz), 5.6–5.8 (m, 1H, crotyl-CH), 5.8–6.0 (m, 1H, crotyl-CH), 7.26 (br dd, 1H, ArH), 7.30 (d, 1H, ArH), 7.55 (br dd, 1H, ArH), 7.8 (d, 1H, ArH). ESI–MS: *m/z* 239.06831 (M + 23), Calc. for $C_{13}H_{12}O_3Na$: 239.06787

(E)-3,3- C-di-crotyl-chromane-2,4-dione (16)

22% yield. ^{1}H NMR (200 MHz $CDCl_3$, p.p.m.) δ: 1.5 (br d, 6H, crotyl-CH_3x2), 2.6–2.9 (br d, 4H, crotyl-CH_2x2), 5–5.3 (m, 2H, crotyl-CHx2), 5.4–5.7 (m, $J = 8.243$ Hz, 2H, crotyl-CHx2), 7.16 (br d, 1H, ArH), 7.3 (d, 1H, ArH), 7.65 (dd, 1H, ArH), 7.95 (dd, 1H, ArH). ^{13}C NMR (50.6 MHz, $CDCl_3$, p.p.m.) δ: 197, 160, 137.01, 130.87, 128.80, 126.83, 126.3, 123.5, 117.53, 41.31, 17.84. ESI–MS: *m/z* 293.0923 (M + 23), Calc. for $C_{17}H_{18}O_3Na$: 293.0923

4-(but-3-enyloxy)-coumarin (17)

47% yield. ^{1}H NMR (200 MHz $CDCl_3$, p.p.m.) δ: 2.7 (m, 2H, buten-CH_2), 4.16 (t, $J = 6.5$ Hz, 2H, buten-CH_2), 5.2 (br d, 2H, buten-CH_2), 5.66 (s, 1H, lactone-H), 5.8–6.0 (m, 1H, buten-CH), 7.25 (br d, 1H, ArH), 7.30 (m, 1H, ArH), 7.55 (br d, 1H, ArH), 7.83 (d, 1H, ArH). ^{13}C NMR (50.6 MHz, $CDCl_3$, p.p.m.) δ: 165.55, 162.96, 153.34, 133.116, 132.01, 123.87, 123.01, 118.11, 116.77, 90.48, 38.30, 32.83. ESI–MS: 239.06737 (M + 23), Calc. for $C_{13}H_{12}O_3Na$: 239.06787

4-(pent-4-enyloxy)-coumarin (18)

64% yield. ^{1}H NMR (200 MHz $CDCl_3$, p.p.m.) δ: 2.0 (m, 2H, penten-CH_2), 2.3 (dd, 2H, penten-CH_2), 4.15 (t, J = 6.3 Hz, 2H, penten-CH_2), 5.0–5.2 (br d, 2H, penten-CH_2), 5.66 (s, 1H, lactone-H), 5.7–6.0 (m, 1H, penten-CH), 7.25 (m, 1H, ArH), 7.33 (m, 1H, ArH), 7.55 (br dd, 1H, ArH), 7.83 (dd, 1H, ArH). ^{13}C NMR (50.6 MHz, $CDCl_3$, p.p.m.) δ: 165.60, 162.94, 153.32, 136.85, 132.31, 123.81, 122.95, 115.74, 111.75, 90.42, 68.48, 29.90, 27.55. ESI–MS: *m/z* 253.08384 (M + 23), Calc. for $C_{14}H_{14}O_3Na$: 253.08352

In silico studies

Docking calculations

The three-dimensional crystal structure of *Taq* DNA polymerase I and Klentaq polymerase employed in this work were obtained from the Protein Data Bank ID code 2KQT. These structures were subjected to energy minimization calculations to remove possible bumps using the Amber12 package. Docking simulations were carried out using AutoDock 4.2 (Morris et al. 2009). In docking experiments, the following parameters were used: the initial population of trial ligands was constituted by 250 individuals and the maximum number of generations was set to 270,000. The maximum number of energy evaluations was 10.0×10^6. All other run parameters were maintained at their default setting. The 3D affinity map was a cube with $50 \times 60 \times 80$ points separated by 0.375 Å and centered on the ddCTP molecule. The resulting docked conformations were clustered into families by the backbone RMSD.

Molecular dynamics

Molecular dynamics simulations and subsequent structural analysis were performed with the Amber12 package. This was used to describe the complexes, whereas the water molecules were represented by using the TIP3P model. Each model was soaked in a truncated octahedral periodic box of TIP3P water molecules. The distance between the edges of the water box and the closest atom of the solutes was at least 10 Å. Sodium ions were added to neutralize the charge of the system. The entire system was subject to energy minimization in two stages in order to remove poor contacts between the complex and the solvent molecules. First, the water molecules were minimized by keeping the solute fixed with harmonic constraint with a force of 100 kcal/molÅ^2. Secondly, conjugate gradient energy minimizations were performed four times using the positional restraints to all heavy atoms of the complexes with 15, 10, 5, and 0 kcal/molÅ^2. The values of RMSD between the initial and minimized structures were lower than 0.5 Å. In the next place, each system was then heated in the NVT ensemble from 0 to 300 K in 500 ps and equilibrated at an isothermal isobaric (NPT) ensemble for another 500 ps. A Langevin thermostat (Izaguirre et al. 2001) was used for temperature coupling with a collision frequency of 1.0 ps^{-1}. The particle mesh Ewald (PME) method was employed to treat the long-range electrostatic interactions in a periodic boundary condition. The SHAKE method was used to constrain Hydrogen atoms. The time step for all MD is 2 fs, with a direct-space, non-bonded cutoff of 8 Å. Finally, the production was carried out at the NPT conditions performing simulations of 30 ns in length for each system. The interactions between inhibitors **6**, **7**, **11** and each residue of *Taq* DNA polymerase I was calculated using the MM/GBSA decomposition program implemented in AMBER 12.

Inhibitor-Residue interaction decomposition: The interaction between inhibitor-residue pairs is approximated by:

$$\Delta G_{\text{Inhibitor}-\text{residue}} = \Delta G_{\text{vdw}} + \Delta G_{\text{ele}} + \Delta G_{\text{GB}} + \Delta G_{\text{SA}} \quad (1)$$

where ΔG_{vdw} and ΔG_{ele} are non-bonded van der Waals interactions and electrostatic interactions between the inhibitor and each *Taq* DNA polymerase I residue in the gas phase. The polar contribution to solvation free energy (ΔG_{GB}) was calculated by using the GB module. ΔG_{SA} is free energy due to the solvation process of nonpolar contribution and was calculated from SASA. All energy components in Equation were calculated using 500 snapshots from the last 5 ns of the MD simulation.

QM/MM setup

The compounds and the side chains of the residues that had at least one heavy atom within 5 Å from the drug molecule (first shell residues) were incorporated into the high-level QM layer. The chosen cutoff value resulted from a compromise between computational cost and efficiency. The remainder part of the system was incorporated into the low-level, relatively inexpensive, MM layer. Only the QM layer was fully geometrically optimized. The QM region was calculated using the M06-2 × /6–31 G(d) method and the MM portion using the AMBER force field. The MM parameters absent in the standard AMBER force field were included from the generalized amber force field (GAFF) (Wang et al. 2004). Atoms in the QM region were optimized using the electrical embedding scheme. Hydrogen link atoms were used to satisfy atoms at the QM and MM interface.

Atoms in molecules theory

After the QM/MM calculation, the optimized geometry for each Inhibitor/DNA polymerase complexes was used as

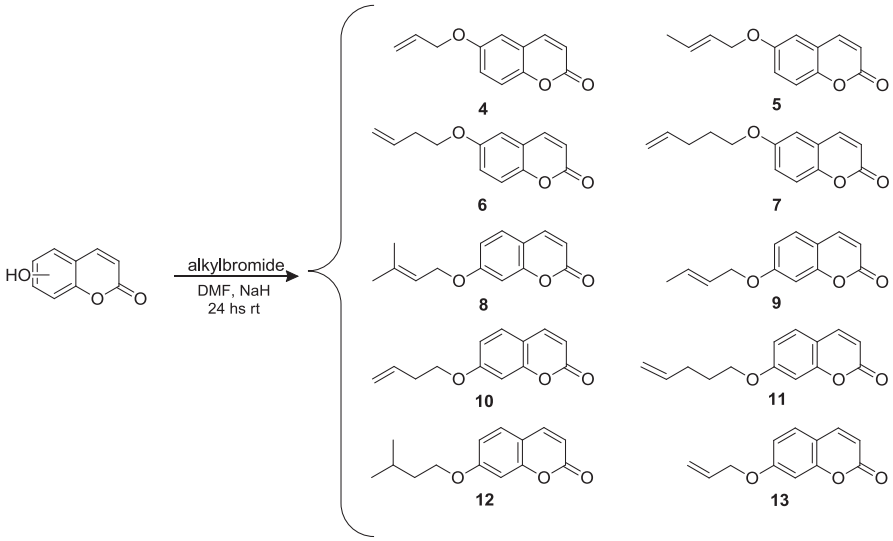

Scheme 1 Synthesis and yields of phenolic derivatives obtained: 6-allyloxy-coumarin (**4**, 75%), 6-crotyloxy-coumarin (**5**, 63%), 6-(but-3-enyloxy)-coumarin (**6**, 60%), 6-(pent-4-enyloxy)-coumarin (**7**, 67%), 7-(*γ*,*γ*-dimethyl-allyloxy)-coumarin (**8**, 84 %), 7-crotyloxy-coumarin (**9**, 85%), 7-(but-3-enyloxy)-coumarin (**10**, 68%), 7-(pent-4-enyloxy)-coumarin (**11**, 61%), 7-(3-methylbutane)-oxycoumarin (**12**, 64%), 7-allyloxy-coumarin (**13**, 70%)

input for quantum theory atoms in molecule (QTAIM) analysis which was performed with the help of Multiwfn software using the wave functions generated at the M06-2 × /6–31 G(d) level. This type of calculations has been used in recent works because it ensures a reasonable compromise between the wave function quality required to obtain reliable values of the derivatives of $\rho_{(r)}$ and the computer power available, due to the extension of the system in study (Vega-Hissi et al. 2015; Gutiérrez et al. 2017).

Molecular biology assays and PCR products analysis

PCR assays

The assayed compounds were dissolved in DMSO. The PCR master mixture consisted of 40 mM Trisacetate *p*H 8.3, 15 mM $MgCl_2$, 2.5 U of *Taq* DNA polymerase (Sigma–Aldrich), 20 mM each oligonucleotide primer, and 2.5 mM each desoxynucleotide triphosphate (dNTP). Inhibition studies were carried out with varying compound concentrations. For inhibition control ddATP at 200 µM concentration was used. All PCRs were done in 20 µL reaction volumes. Genomic DNA for *β*-tubulin from *Aspergillus parasiticus* was used as template. The sequence of the sense primer was 5′-GGT AAC CAA ATA GGT GCC GCT-3′, and the antisense primer was 3′- TAG GTC TGG TTC TTG CTC TGG ATG-5′. A complementary sense primer 5′-CAT CCA GAG CAA GAA CCA GAC CTA-3′ was also used. Thermocycling conditions consisted of 35 cycles of denaturation at 95 °C for 1 min followed by primer annealing at 56 °C and primer extension at 72 °C for 90 seg. After completion of reaction, 2 µl of loading buffer 10× (0.25% of bromophenol blue, 0.25% xylene cyanol FF, 15% Ficoll 400 in water) were added. The amplified DNA sequences were electrophoresed for 60 min. in 0.8% agarose gel in buffer TBE 1× (Tris-boric-EDTA, pH: 8) at 75–80 V using TBE running buffer 1×. Finally, gels were stained using 0.5 µg of ethidium bromide per ml. Amplified DNA bands were detected visually with UV transilluminator. Each assay was replicated between three and seven times.

Analysis of PCR products

The relative intensities of ethidium bromide stained PCR products were analyzed by using the optical scanner and the image program. The image of stained agarose gels was captured using a Photodocumentator UVP Imaging System. The digitized band images were processed using the Image processing program (Scion Image, public domain program) and the IC_{50} values were determined by the GraphPad Prism program.

Results and discussion

Chemistry

We used 6-hydroxy (**1**), 7-hydroxy (**2**) and 4-hydroxycoumarin (**3**) as substrates, to obtain a homologous series of derivatives in whose structure only subtle changes occur by employing different alkene halides such as: 4-pentene, 3-butene, *trans*-crotyl, *γ*,*γ*-dimethyl and allyl bromide and 1-bromide-3-methylbutane (Scheme 1). These specific changes in the side chain are valuable for establishing structure/activity relationships.

Different yields and rates of reaction for the same alkyl halide between 6-hydroxycoumarin (**1**) and 7-hydroxycoumarin (**2**) were observed, indicating a difference in the nucleophile quality. For example, using soft mass fragmentation methods (ESI-MS) product **11** showed

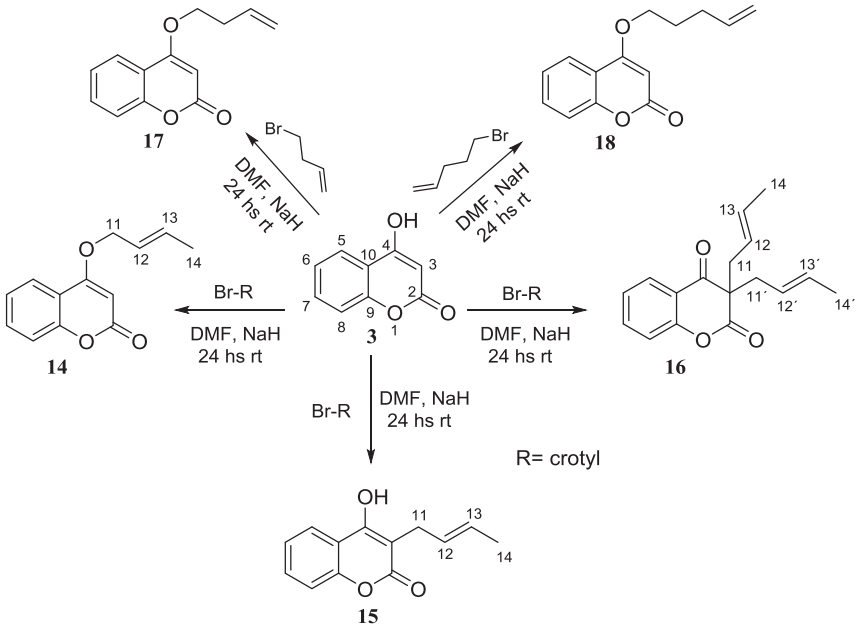

Scheme 2 Alkylated derivatives obtained using the enolic 4-hydroxycoumarin (**3**) as substrate: 4-*O*-crotyloxy-coumarin (**14**, 41%), 4-hydroxy-3-*C*-crotyl-coumarin (**15**, 30%), 3,3-*C*-di-crotyl-chromane-2,4-dione (**16**, 22%) in the same reaction. 4-(but-3-enyloxy)-coumarin (**17**, 47%), 4-(pent-4-enyloxy)-coumarin (**18**, 64%) separately

different fragments from those of its "structural sibling" **7**. The analysis shows a different degree of polarization in the phenolic Carbon-Oxygen bond, since the loss of the alkyl group is not observed in **11**. The complete loss of the alkyl group in **7** indicates the different bond strength, which is susceptible to ionization by a soft method (Figures 7.1 and 11.1 supporting material). Undoubtedly, this reactivity difference appears in the dissimilar electron densities shown by C-6 and C-7 atoms (Fig. 1 supporting material). It seems that C-6 has higher double bond aromatic nature, unlike the positive partial charge in C-7, conferring a better nucleophile character to 6-hydroxycoumarin. Now, using (*E*)-crotyl bromide, we could notice the appearance of new signals in the ^{1}H NMR spectrum (Figs. 5.2, 9.2, 14.2 and 15.2 supporting material: red circle denotes duplicate signals) due to a possible *cis*/*trans* coupling. Best yields were obtained for crotyl and γ,γ-dimethylallyl derivatives, where conjugation stabilizes an allylic carbocation with $\pi-$bonds delocalized.

Instead, using 4-hydroxycoumarin (**3**) and (*E*)-crotyl bromide we obtained three different products in the same reaction, suggesting a higher reactivity of **3** than 6-hydroxycoumarin (**1**) or 7-hydroxycoumarin (**2**) (Scheme 2).

We propose a disubstituted *C*-alkylated product **16** at position three, mainly by the duplication of proton signals compared with **15** (*C*-alkylated mono-substituted), now in a sp^3 Carbon instead of the original sp^2, therefore migrating H-11 signals to higher fields (3.45 to 2.7 p.p.m.). Even the ^{13}C NMR spectra show the signal attributable to C-11 at 41.31 p.p.m. The *O*-alkylated derivative **14** was the second polar product, and the pattern of signals is similar to those of a *C*-alkylated mono-substituted derivative **15**. We could notice that, when the alkyl group is bonded to another Carbon atom (**15**) the Ms/Ms analysis showed a stable cation allylic loss, originating a progenitor fragment of 175 *m/z*. In contrast, *O*-alkylated product (**14**) lost the crotyl group completely, instead of allylic moiety due to the high polarizability degree present in the labile Oxygen-Carbon bond (Figs. 3.A, 14.1, and 15.1 supporting material). The *O*-alkylated derivative **14** obtained from the enol-coumarin (**3**) was the expected one in a typical substitution mechanism, where the enolic hydroxyl is able to displace the bromine atom. However, for *C*-alkylated products, C-3 could act as nucleophilic atom displaying halogens. Moreover, keto form of α-carbonyl systems showing some acidity degree, and the Hydrogens located at this position have the potential to make a carbanion in C-3 (Fig. 3.B supporting material) (Garro et al. 2015c). Finally, performing reactions with 4-pentene and 3-butene bromide, only *O*-alkylated products were synthesized (Scheme 2). Interestingly, no *C*-alkylated derivatives were observed, indicating a different reactivity when allylic kind compounds cannot be formed (for complete spectroscopy data of **4**–**18** see the supporting material). Finally, in our knowledge, compounds **6**, **7**, and **16** have not been previously described in bibliography.

Molecular Biology assays

The potential anti-cancer therapeutic properties of the obtained alkenylcoumarins was evaluated. The family of compounds was screened by polymerase chain reaction (PCR) inhibition. PCR allows to find new polymerases inhibitors comparing the absence of enzyme activity using known inhibitors such as 2', 3' dideoxynucleotides

(ddNTPs). Human DNA polymerases share the same activity and a right hand shape with *Taq* DNA polymerase. Due to the high degree of structural conservation between these proteins, PCR can be used in the search for new antitumoral agents (Pungitore 2014). Results revealed that analogs **6**, **7** showed inhibitory activity and **11** showed a little activity, with IC_{50} values of 76.16 ± 1.25; 48.33 ± 2.85 and 187.30 ± 4.27 μM, respectively (Table 1). IC_{50} values lower to 200 μM are considered active in "in vitro" PCR inhibition assays (Mizushina et al. 2005).

The search for the moieties involved in enzyme recognition clearly highlights the lineal alkene functionalization at the aromatic ring. For this reason, alkoxy derivatives (**6**, **7**, and **11**) that showed these group at coumarin positions six and seven proved to be experimentally active. Possibly, such activity consists of the greater hydrophobicity and flexibility present in this moiety, in contrast to the other shorter or branched alkyl groups. Furthermore, the structural isomer group of pentene "$\gamma,\gamma-$dimethylallyl" and the alkane derivative 3-methylbutane (which also has five Carbon atoms) were inactive; perhaps giving an idea of the kind of non-bulky hydrophobic groups involved into the protein recognition. It is apparently a necessary condition that these alkyls are present on the aromatic Oxygen atoms, since the substituted derivative at position four of coumarin (enolic Oxygen) turned out to be inactive. Furthermore, five derivatives previously obtained using$\square\gamma,\gamma-$dimethylallyl and allyl bromide with 4-hydroxycoumarin (**3**) were also inactive against *Taq* DNA polymerase (Garro et al. 2014a). It might even be thought that the different values of activity between pentenyl-oxy isomers **7** and **11** (48.33 ± 2.85 μM and 187.30 ± 4.27 μM, respectively) may be due to the different electron density present at the six and seven positions of coumarin, which was determined by Electrospray fragmentations (ESI-MS). A similar analog in terms of chemical reactivity and flexibility of pentenyl-oxy would be the butenyl-oxy moiety, only with one methylene group less. Butenyl-oxy products were active when located only at position six of coumarin (**6**), but not at position seven (**10**) or four (**17**), indicating the importance of charge electronic density of coumarin core at this position. Moreover, in a previous study (Garro et al. 2014a) we demonstrated that 6-hydroxycoumarin (**1**) was inactive against *Taq* DNA polymerase. Furthermore, a linear and flexible group with alkene end function at C-6 seems to be a condition for biological activity, because the isochemical (but allylic) crotyl-oxy group (**5**) of butenyl-oxy was not active. Finally, the maximum value of activity (IC_{50} = 48.30 ± 2.85 μM) reached by product **7** could be added to the application of pentenyl-oxy group at C-6 of coumarin as a possible candidate molecule for further studies. To elucidate a probable binding site and the interactions of protein/alkenylcoumarins complexes we performed in silico calculations.

Table 1 Inhibitory activity and IC_{50} values for the compounds 6, 7, and 11

Compounds	[a]IC_{50} values
6-(but-3-enyloxy)-coumarin (**6**)	76.16 ± 1.25
6-(pent-4-enyloxy)-coumarin (**7**)	48.33 ± 2.85
7-(pent-4-enyloxy)-coumarin (**11**)	187.30 ± 4.27

[a]IC_{50} values were determined by interpolation from plots and enzyme activity vs. inhibitor concentration. The IC_{50} values are means from at least five independent experiments and standard deviation never exceeded 7%. The results are expressed in μM. The rest of assayed compounds have shown values higher than 200 μM (results not shown) and considered inactive

In silico studies

First, all compounds were blind docked with the complete Klentaq DNA polymerase structure using "random seed" variant (for calculation times reasons). Then, we made a site-directed study within the active site. Both procedures were performed with the presence of DNA fragment, obtaining similar results for all cases (Fig. 3.C supporting material). Despite the lack of structural homology with the natural polymerase substrates, all compounds tested were located within the catalytic site (Fig. 1).

Besides, with a more refined method, the three biological active compounds were docked in the active site of *Taq* DNA polymerase I structure. Figure 4.A in the supporting material shows a summary of the molecular docking results. The receptor molecule used in this study was the open

Fig. 1 Binding of compound **7** within the polymerase catalytic active site

conformation of this protein co-crystallized in the presence of a short DNA fragment and a ddCTP (di-deoxy-cytidine triphosphate) molecule (PDB code 2KTQ) (Martin et al. 2011). Here are plotted the number of conformations from each cluster and the leader energy binding (red numbers) for all compounds, selecting the leader of the most populated cluster for further studies. In order to elucidate the dynamic features of the coumarin/polymerase complexes binding after docking calculations, their structures were refined by performing Molecular Dynamic Simulations. Figure 4.B in the supporting material shows the temporal evolution of the root mean square deviations (RMSD) of the polymerase backbone atoms relative to the docking structure. First the RMSD values increased quickly because the structure of complexes relaxes and removes the repulsion within systems. After two nanoseconds of simulations, the systems reached the equilibrium state and the average RMSD values were 2.04 (SD = 0.27), 1.90 (SD = 0.17) and 1.93 (SD = 0.20) for compounds **6**, **7**, and **11**, respectively. These low standard deviation values (< 0.3 Å) indicate that the molecular dynamics simulations stabilities for the three complexes are reliable. These spectra suggest that the interactions between compounds **6**, **7**, and **11** with *Taq* DNA polymerase I are almost the same and reflect their similar binding modes. Besides, Fig. 2 indicates that compounds **7** and **6** are forming strong interactions with the three DNA nitrogenous bases DC111, DG204, and DG205. Furthermore, compound **11** shows weaker DNA interaction than **7** or **6** (only with DC111 and DG205). Maybe, lower DNA recognition offers less biological activity (187.30 ± 4.27 μM).

At first, the binding between inhibitors and DNA fragment, added to the planarity of coumarins, invites us to think that they have strong interactions (probably by efficient $\pi-$stacking and other minor interactions between aromatic coumarin moiety with DNA chain). On the other hand, residues Gln613, Ile614, Leu670, Tyr671, Gln754, and His784 are responsible for recognizing **6**, **7**, and **11** coumarin derivatives, but only **7** (the most powerful inhibitor) shows a strong interaction with Glu615.

Finally, we used QTAIM technique to decompose global interactions on atoms or atoms group contributions

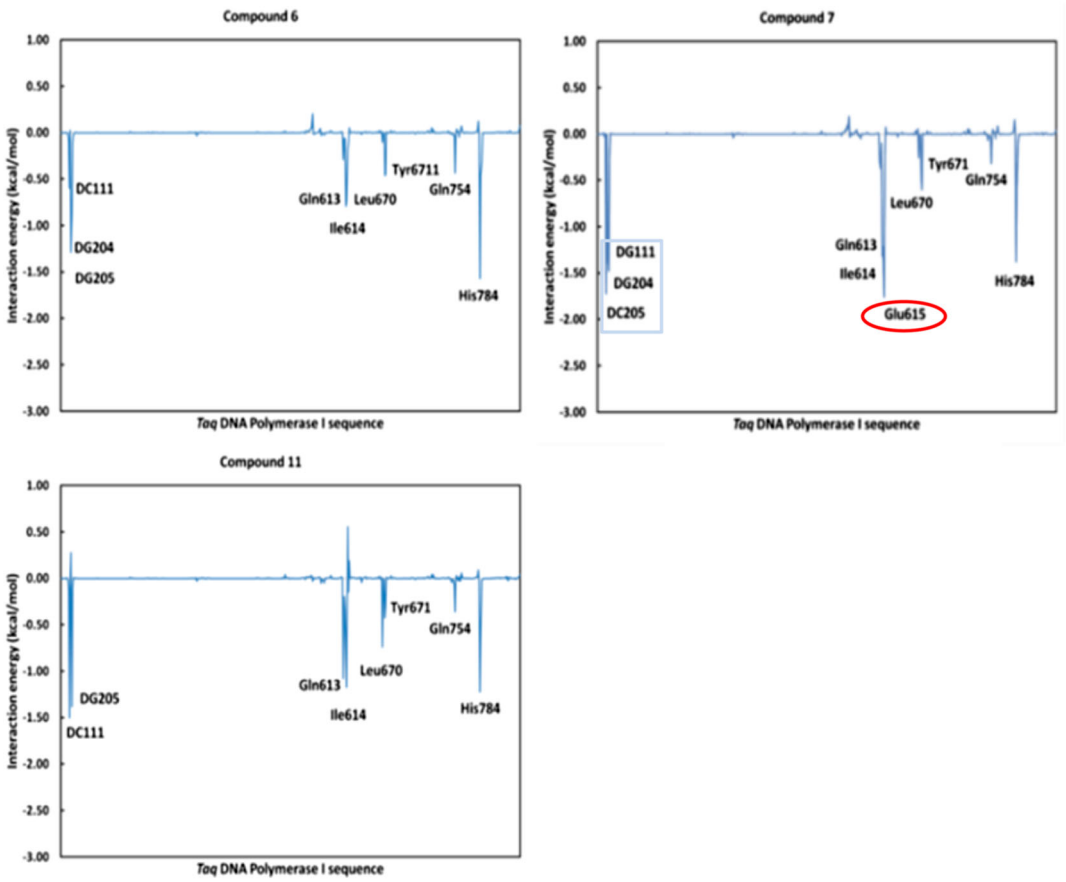

Fig. 2 Inhibitor/residue and inhibitor/DNA interaction spectra of (**a**) polymerase/**6**, (**b**) polymerase/**7**, and (**c**) polymerase/**11** according to the MM-GBSA method. The *x*-axis denotes the residue number of *Taq* DNA polymerase I and the *y*-axis denotes the interaction energy between the inhibitor and specific residues or nucleotides. Red circle denotes the strong interaction of compound **7** with Glu 615. The light blue square denotes the interactions of **7** with DNA (DG DNA guanine, DC DNA cytosine)

(functional group), to analyze the ligand molecule optimization. However, for the QTAIM analysis to be reliable, good geometry is needed. For this reason, the most representative structure was taken from the molecular dynamics path for each inhibitor/polymerase complex. It was performed using the cluster tool implemented in the Amber12 simulations package. Then, each representative structure was optimized at M06-2 × /631 G(d) level using QM–MM calculations. Accordingly, for the QTAIM analysis we partitioned the compounds into two substructures (Fig. 3).

Figure 4 shows, in stacked bars, the sum of charge density values at the intermolecular bond critical points for complexes of compounds **6**, **7**, and **11** with polymerase.

As depicted in Fig. 4, the sum of charge density for compound **7** is the highest, indicating that it is the most active compound presented in this paper. Furthermore, this is in accordance with our experimentally IC_{50} values obtained. Moreover, it shows that the interaction strength of the coumarin scaffold differs within the active site, depending on the kind and position of the substituent. This can be clearly seen by analyzing the height of the blue bars in Fig. 4 for compounds **7** and **11**. Both compounds have the same substituent (4-pentenyl-oxy group), but in compound **7** the coumarin nucleus interacts with more force than **11** when the 4-pentenyl-oxy moiety is located at position seven. This clearly shows different electronic densities between structural isomers **7** and **11**, consistent with the ESI mass fragmentation studies and resonance method described before. On the other hand, compound **6** is formed by the coumarin core substituted at C-6 and the shorter 3-butenyl-oxy group (showing a methylene group less). As in compound **7**, the interaction force between the coumarin nucleus and the polymerase active site is greater than compound **11**. These results clearly indicate that the inhibitory strength of these compounds is mostly related to the coumarin core and his electronic density.

To understand the different binding modes, present in the coumarin core in compounds **6**, **7**, and **11**, Fig. 4.C in the supporting material shows the sum of charge density values at the intermolecular bond critical points (only for coumarin moiety). Although the binding mode is similar, a clear difference is observed in the strength of dipolar interactions with Glu615 residue. Aspartic and Glutamic are conserved acidic residues in DNA polymerases and they are essential for the catalytic function (for example binding magnessium ions). Figure 5 shows the spatial view for **6**, **7**, and **11**.

It can be observed that the coumarin core presents different modes of binding, according to the position and kind of substituent group. In turn, for compounds **6** and **11**, the coumarin core moves away from the Glu615 residue, decreasing the interaction with this pivotal residue in the polymerase active site. Furthermore, carbonyl function in **7** could be also responsible for the greater interaction between

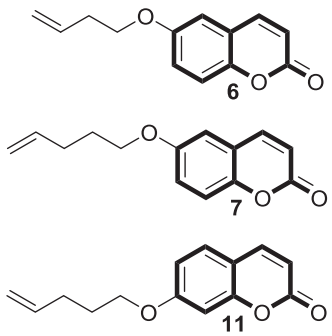

Fig. 3 Molecular structures of coumarin inhibitors. Coumarin core sub-structure is shown in solid bonds

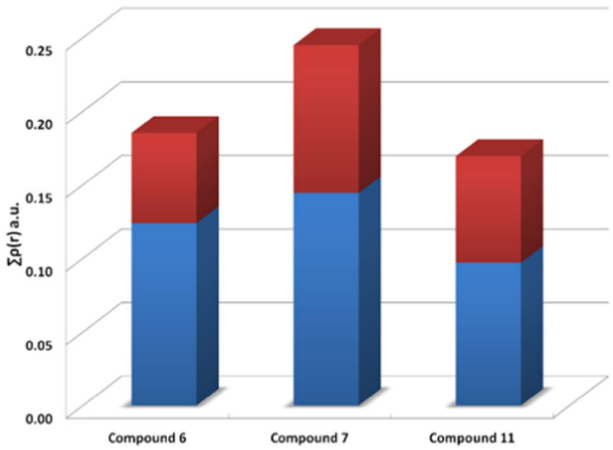

Fig. 4 The contribution of the coumarin core to the overall anchoring strength of compounds at the receptor binding pocket is depicted in blue bars, while the contribution of the different substituents is shown in red

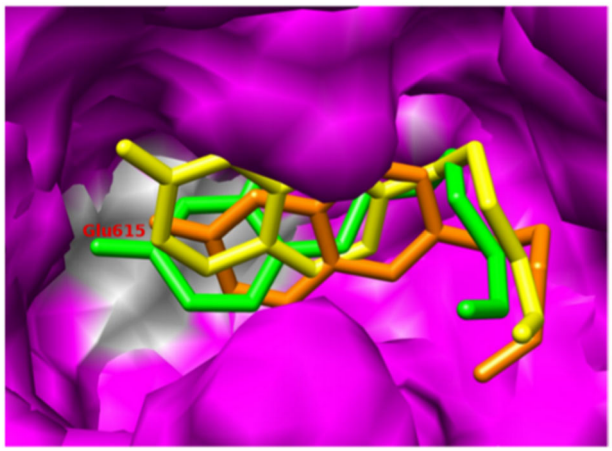

Fig. 5 Backbone superposition of compounds **6** (sticks orange), **7** (sticks green), and **11** (sticks yellow) inside *Taq* DNA polymerase I (magenta surface). Only some structural elements in the superposition are shown for easy viewing

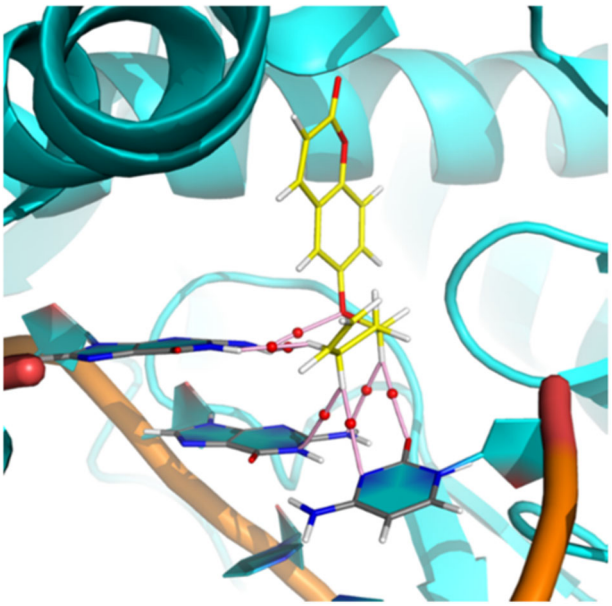

Fig. 6 Molecular graph of the noncovalent interactions between the nitrogenous bases DC111, DG204, and DG205 with compound **7** (yellow sticks). The elements of the electron density topology are shown. The bond paths connecting the nuclei are represented in pink sticks and the bond critical points are shown as red spheres

coumarin core with Glu615, probably due to the different negative electronic density that this carbonyl presents respect to **6** and **11**, previously described.

From the standpoint of the substituents, Fig. 4 clearly shows that compound **7** presents the strongest interactions. Finally, Fig. 6 shows the network of physicochemical interactions of 4-pentenyl-oxy group of **7** within polymerase binding pocket. The molecular graphs show large number of noncovalent interactions with nitrogenous DNA bases, which are key for the inhibitory activity of product **7**.

Furthermore, Fig. 6 shows the proximity of the carbonyl moiety of **7** with the α-helix portion that includes Glu615 residue.

Conclusion

Using a simple and feasible method we prepared related alkenylcoumarins using three non-active substrates. In order to achieve a more rational design, we made products that showed subtle chemical variations, like hydrocarbonated long chain, polarity, olefin position and linear or branched groups. Only phenolic coumarins substituted by linear alkenes were active, preferably at position six. The coumarin nucleus seems to contribute even a little more than alkenyl-oxy groups to enzymatic recognition; however, we showed in a previous work (Garro et al. 2014a, 2014b) that neither coumarin nor 6-hydroxycoumarin alone can inhibit *Taq* DNA polymerase. The coumarin nucleus would be necessary for internalization within the active site. However, the recognition of Glu615 residue by the **7** inhibitor would be clearly crucial to its greater activity. For this reason, we propose pentenyl-oxy at position six of coumarin as a potential structure for further studies in the search of pharmacophores for new coumarin antitumoral agents.

Acknowledgements This research was supported by CONICET (PIP 00360) and UNSL (PROICO 02/2516). EFB thank CONICET for doctoral fellowship. HAG thank for post-doctoral position in the Max Planck Laboratory for Structural Biology, Chemistry, and Molecular Biophysics of Rosario (MPLbioR). We wish to thank to Lic. M. Ferrari, Dr. C. Ardanáz, and Dr. G. Labadie for their help. Also, we wish to thank to Dra. C. García and Prof. V. Martín from IUBO (Spain) for their help in the use of HRMS. We wish specially thank to Drs. L. Mascotti and M. Juri-Ayub for DNA material gently provided. We appreciate revision of the manuscript by staff from the "Instituto de Lenguas, Universidad Nacional de San Luis". This work is a part of the doctoral thesis of EFB.

Compliance with ethical standards

Conflict of interest The authors declare that they have no conflict of interest.

References

Bernauer J, Janin J, Poupon J (2007) A new protein–protein docking scoring function based on interface residue properties. Bioinformatics 23:555–562

Garro HA, García C, Martín VS, Tonn CE, Pungitore CR (2015a) A new iridoid, verbascoside and derivatives with inhibitory activity against *Taq* DNA polymerase. Bioorg Med Chem Lett 25:914–918

Garro HA, Pungitore CR (2015b) Coumarins as potential inhibitors of DNA polymerases and reverse transcriptases. Searching new antiretroviral and antitumoral drugs. Curr Drug Discov Technol 12:66–79

Garro HA, Manzur MJ, Ciuffo GM, Tonn CE, Pungitore CR (2014a) Inhibition of reverse transcriptase and *Taq* DNA polymerase by compounds possessing the coumarin framework. Bioorg Med Chem Lett 24:760–764

Garro HA, García C, Martín VS, Tonn CE, Pungitore CR (2014b) Chemistry and biological activity of coumarins at molecular level. Nat Prod Comm 9:1091–1094

Garro HA, Petroselli G, Pungitore CR, Tonn CE, Erra-Balsells R (2015c) Synthesis and characterization of conjugated olygomers by acetone self-condensation end-functionalized with 4-hydroxycoumarin. J Mater Environ Sci 6:1137–1141

Ghiano DG, de la Iglesia A, Liu N, Tonge PJ, Morbidoni HR, Labadie GR (2017) Antitubercular activity of 1,2,3-triazolyl fatty acid derivatives. Eur J Med Chem 125:842–852

Gutiérrez LJ, Angelina E, Gyebrovszki A, Fülöp L, Peruchena N, Baldoni HA, Penke B, Enriz RD (2017) New small-size peptides modulators of the exosite of BACE1 obtained from a structure-based design. J Biomol Struct Dyn 35:413–426

Izaguirre JA, Catarello DP, Wozniak JM, Skeel RD (2001) Langevin stabilization of molecular dynamics. J Chem Phys 114:2009–2014

Kostova I (2007) Biologically active coumarins as inhibitors of HIV-1. Futur. HIV Ther 1:315–329

Kostova I, Genova P, Argirova R (2006) Structure-activity relationships of synthetic coumarins as HIV-1 inhibitors. Bioinorg Chem Appl 1:1–9

Li B (2012) Protein docking prediction using predicted protein-protein interface. Bioinformatics 13:1–17

Liu R, Li X, Lam KS (2017) Combinatorial chemistry in drug discovery. Curr Opin Chem Biol 38:117–126

Martin OA, Garro HA, Kurina-Sanz MB, Pungitore CR, Tonn CE (2011) In silico study of the inhibition of DNA polymerase by a novel catalpol derivative. J Mol Model 17:2717–2723

Mizushina Y, Akihisa T, Ukiya M, Hamasaki Y, Murakami-Nakai C, Kuriyama I, Takeuchi T, Sugawara F, Yoshida H (2005) Structural analysis of isosteviol and related compounds as DNA polymerase and DNA topoisomerase inhibitors. Life Sci 77:2127–2140

Morris GM, Huey R, Lindstrom W, Sanner MF, Belew RK, Goodsell DS, OlsonAJ (2009) Autodock^4 and AutoDockTools^4: automated docking with selective receptor flexibility. J Comput Chem 16:2785–2791

Olmedo D, Bedoya LM, López-Pérez JL, Del Olmo E, Muñoz E, Alcamí J, Gupta MP, San Feliciano A (2012) 3-Phenylcoumarins as inhibitors of HIV-1 replication. Molecules 17:9245–9257

Pungitore CR (2014) Natural products, synthetic and non-nucleoside compounds as inhibitors of enzymes related to DNA: Update 2013. Curr Enzym Inhib 10:13–38

Rayati S, Nejabat F (2016) Catalytic properties of the homologous series of the β-brominated-pyrrole manganese(III) tetraphenylporphyrins. Polyhedron 104:52–57

Stefanou V, Melagraki G, Afantitis A, Athanasellis G, Igglessi-Markopoulou O, McKee V, Markopoulos J (2011) Functionalized 4-hydroxy coumarins: novel synthesis, crystal structure and DFT calculations. Molecules 16:384–402

Vega-Hissi E, Tosso R, Enriz RD, Gutiérrez LJ (2015) Molecular insight into the interaction mechanisms of inhibitors (R)-1t and (S)-1m with BACE1 protease: QM/MM investigations. Int J Quantum Chem 115:389–397

Venugopala KN, Odhav B (2013) Review on natural coumarin lead compounds for their pharmacological activity. J Biomed Biotechnol 1:2–14

Wang J, Wolf RM, Caldwell JW, Kollman PA, Case DA (2004) Development and testing of a general amber force field. J Comput Chem 25:1157–1174

Wijkmans JC, Beckett RP (2002) Combinatorial chemistry in anti-infectives research. Drug Discov Today 7:126–132